The Report Committee for Daniel William Corona
Certifies that this is the approved version of the following Report:

Evaluating Piezoelectric Constant d_{31} of Films Deposited on Silicon Using Low Frequency-Actuated Piezoelectric Cantilever Structures

APPROVED BY
SUPERVISING COMMITTEE:

Neal A. Hall, Supervisor

Michael Haberman

Evaluating Piezoelectric Constant d_{31} of Films Deposited on Silicon Using Low Frequency-Actuated Piezoelectric Cantilever Structures

by

Daniel William Corona

Report

Presented to the Faculty of the Graduate School of

The University of Texas at Austin

in Partial Fulfillment

of the Requirements

for the Degree of

Master of Science in Engineering

The University of Texas at Austin

December 2018

Abstract

Evaluating Piezoelectric Constant d_{31} of Films Deposited on Silicon Using Low Frequency-Actuated Piezoelectric Cantilever Structures

by

Daniel William Corona, MSE

The University of Texas at Austin, 2018

Supervisor: Neal Hall

Piezoelectric coefficients of films deposited on silicon are surprisingly expensive to measure using experiments commonly found in literature. A low-cost method of approximating the small-signal piezoelectric coefficient d_{31} for a film by comparing data from a single laser-doppler vibrometer measurement and a numerical model is presented. This method is useful for directly evaluating the quality of a piezoelectric film. Relevant properties of piezoelectric materials are introduced, and pitfalls of prior testing methods are discussed. An analytical model of the test is developed to provide insight into critical test parameters. The test is validated by comparing the numerical and the analytical model, by comparing experimental results to film x-ray diffractometry measurements, and by building opportunities for validation into the experiment. Explicit experimental validation is deemed too expensive and unnecessary for the immediate needs of the author. The method is also applied to evaluate the piezoelectric properties of several AlN films developed using varying fabrication parameters. Results are used to improve the fabrication process of an AlN film on silicon for use in piezoelectric sensor prototypes.

Table of Contents

List of Tables

List of Figures

I. INTRO/BACKGROUND

a. Piezoelectric materials

A piezoelectric material is one that, when subjected to an electric field, converts some of the electrical energy to mechanical energy, causing deformation of the material. With the exception of loss due to friction during deformation and dielectric loss, this is a reversible process. In other words, when a piezoelectric material is deformed, some strain energy in the material is converted to electrical energy, yielding a measurable voltage across the material. The piezoelectric effect is commonly utilized in sensors and actuators. These include microphones with high signal-to-noise ratio, speakers and buzzers, and positioners capable of nano-scale precision. These materials are also used in oscillators (i.e. high frequency clocks), filters, and high-voltage power sources, though these applications are not discussed in detail in this report. Well-known examples of piezoelectric materials include Lead-Zirconate Titanate (PZT), Quartz, Barium Titanate ($BaTiO_3$), and Aluminum Nitride (AlN).

THE PIEZOELECTRIC EFFECT

The piezoelectric effect is caused by a charge dipole moment within the material, which is due to charge asymmetry within a unit cell of the crystal structure. For some materials, including PZT, the direction of the dipole within each unit cell is unpredictable. When dipoles face in different directions, the magnitude of their vector sum is less than the vector sum of aligned dipoles, so the overall piezoelectric effect is reduced. These materials must be "poled" by applying a high electric field at high temperature, aligning all dipoles to yield a macroscopic piezoelectric effect. For other materials, including AlN, the direction and alignment of dipoles is purely dependent on the orientation of the crystal structure and other deposition conditions, so no poling is needed. When a piezoelectric material is strained in the direction of a dipole, charges are pulled further apart in space, increasing the dipole moment, yielding a change in electric

potential across the material. Conversely, when an electric potential is applied, electrostatic attraction and repulsion of the charges causes a strain in the material.

PIEZOELECTRIC COEFFICIENT MATRICES

Though significant nonlinearity can occur when large signals are encountered, electromechanical transduction in these materials is generally assumed to be linear for small strains and charges. These linear relationships are described for a 3-dimensional material by a set of piezoelectric constitutive equations commonly found in textbooks on piezoelectric devices [1]. The equations involve piezoelectric coefficient matrices *d*, *e*, *g*, and *h* alongside material property matrices representing stiffness and dielectric constant tensors. (1) and (2) provide examples of these equations. In sensor and actuator applications, piezoelectric constants are a crucial figure of merit for piezoelectric films because these determine the efficiency with which input mechanical energy can be converted into a signal or vice versa.

$$S = s^{E}T + dE \tag{1}$$

$$D = dT + \varepsilon^{T}E \tag{2}$$

When a material is strained in one direction, the Poisson effect dictates that proportional strain (determined by Poisson's ratio for that material) also occurs perpendicularly. Because of this, *d*, *e*, *g*, and *h* can be defined by matrices with components relating strain along one axis to electric field along another axis. A charge dipole also experiences a net shear force when exposed to a perpendicular electric field, so shear strains can also be related to electric fields perpendicular to the dipole axis. These relationships yield 3 primary components of this tensor: 33, 31 and 15, where the indices of these elements correspond to the direction of the electric field/charge and the direction of stress/strain respectively as shown in figure 1. These are the most common values reported in literature. For transversely isotropic materials (most piezoelectric films), electromechanical coupling can be specified accurately using only these 3 components in a matrix as shown in (3) [2].

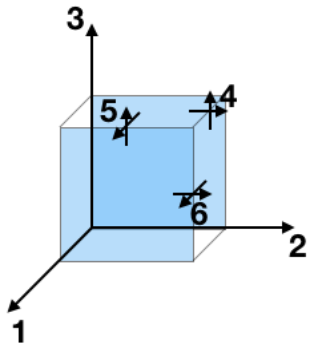

Figure 1: Axes represented by piezoelectric coefficient and material property matrix indices

$$d=\begin{bmatrix} 0 & 0 & 0 & 0 & d_{15} & 0 \\ 0 & 0 & 0 & d_{15} & 0 & 0 \\ d_{31} & d_{31} & d_{33} & 0 & 0 & 0 \end{bmatrix} \quad (3)$$

d, *e*, *g*, and *h* describe the same piezoelectric effect, but account for dielectric permittivity and stiffness of the material differently. Because of this, if stiffness, dielectric permittivity, and a single piezoelectric coefficient matrix is known, then the other three matrices can be derived. For example, shown in (4), the *e* coefficient matrix can be easily calculated directly from *d* and the short-circuit stiffness matrix C^E [2].

$$[e]=[C^E][d] \quad (4)$$

b. AlN

USES

Despite its marginal piezoelectric coupling compared to other materials like PZT, AlN is commonly used in sensor applications including MEMS pressure sensors, accelerometers, and microphones due to its extremely low dielectric loss factor, low dielectric permittivity, and robustness to extreme temperatures. Signal-to-noise ratio, an important figure of merit for many MEMS sensors, is directly affected by the value of the applicable piezoelectric coefficients relative to sources of noise including the material's dielectric loss [3].

CRYSTAL STRUCTURE/MATERIAL PROPERTIES

AlN is a III-V nitride with wurtzite crystal structure. Like other wurtzite materials like ZnO and GaN, the AlN unit cell exhibits a charge dipole normal to the (0002) plane (i.e. along the c-axis) due to its lack of inversion symmetry about this plane. Because of this, maximum piezoelectric coupling occurs when AlN is grown in (0002) orientation. Symmetries in AlN's hexagonal structure make it a transversely isotropic material. A diagram of AlN's crystal structure is shown in figure 2.

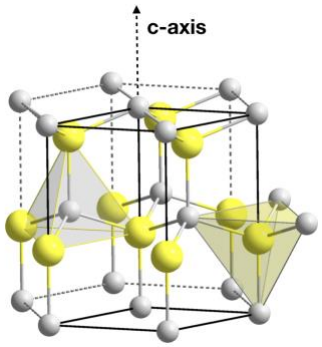

Figure 2: Diagram of AlN's Hexagonal Wurtzite Crystal structure showing c-axis (0002) orientation. Yellow points correspond to N atoms, while gray points correspond to AlN [4].

Reported properties for quality AlN films are shown alongside coefficients for other common piezoelectric materials in table 1 [5].

Material	**d_{31} [pm/V]**	**d_{33} [pm/V]**	**d_{15} [pm/V]**	**tan δ**	**ε_{11}^{s}[C/V]**	ε_{33}^{s}[C/V]
AlN	-2.65	5.09	4.07	0.002	9	10.7
PZT-5H	-274	593	741	0.04	1710	1430
PZT-5A	-171	374	584	0.02	919	827

Table 1: Table of reported AlN and PZT piezoelectric and dielectric properties

SPUTTER DEPOSITION PROCESS/DIFFICULTIES

AlN films can be deposited using pulsed laser deposition, molecular beam epitaxy, chemical vapor deposition, or reactive ion plasma sputtering. In this work, the test is applied to characterize films deposited by reactive plasma sputtering. For this process, a metal seed layer (Ti, Pt, etc.) is deposited, which acts as a bottom electrode for the film and helps to orient crystal growth. The sputtering step is then carried out by placing an aluminum sample, the "target," a short distance from the wafer surface on which the film will be deposited and exposing the target to a plasma of high mass Ar+ ions and reactive N- ions. The Ar+ ions bombard the surface of the target, causing Al+ ions to be sputtered from the surface and collide with the wafer surface. In this high energy state, Al+ ions react with N- to form AlN with orientation, film stress, and purity controlled by the kinetic energy of the sputtered particles, the amount of N- in the plasma, and the seed material on the wafer, among many other factors. Because this process is affected nonlinearly by many interrelated parameters, there is no universally accepted deposition configuration, and any change in equipment requires adjustment of parameters including temperature, pressure, target-to-wafer distance, applied power, N-/Ar+ flow rate, and seed layer properties before quality, properly oriented AlN film can be achieved. Many depositions are necessary when developing a deposition process, so simplifying other steps involved in the test wafer fabrication is crucial [6], [7].

Though not a comprehensive list, the two primary characteristics of a film which can significantly degrade piezoelectric coupling are:

> ***Crystal structure mis-orientation****:* the presence of the (0002) crystal orientation versus other orientations should be maximized to yield maximum piezoelectric coupling. X-ray diffractometry (XRD) measurements provide provides a reliable measurement of the presence of crystal orientations. While (0002) orientation is a requirement for a quality film, one cannot confirm that a film has the expected piezoelectric constants without directly testing for them. Even films that appear to yield near-ideal crystal orientation results can yield poor coupling coefficients

when XRD data is misinterpreted or other quality issues occur that are not revealed by these measurements.

Defects: Defects can manifest as pockets of either of the above issues, or as holes in the film. Minor defects can affect coupling, while major defects can short the bottom and top electrodes, ruining devices.

There are several other important measures of piezoelectric film quality which can be determined easily. Film thickness uniformity across a wafer affects the yield of quality devices on a wafer after fabrication, since devices are generally designed for a given thickness. Stress in the film is important when film stress effects the dynamics of a device. Film stress can deform devices and in extreme cases causes cracking of deposited films, destroying most devices on a wafer. These properties can be easily measured using other methods not discussed in this report. Film impedance, determined by dielectric loss (real) and permittivity (complex), is also important. Dielectric loss, in particular, contributes to the intrinsic noise of a sensor, which reduces signal-to-noise ratio. These properties, including piezoelectric coefficients, can vary across a single wafer as film quality changes, often necessitating measurement of film quality at multiple points on the wafer.

c. Other tests/primary testing challenges

Several test methods have been proposed for determining the piezoelectric coefficients of films. While some provide measurements with good reported repeatability, most manage only general estimates, and none offer the efficiency, simplicity, and precision necessary for quickly comparing results of many AlN depositions during a process optimization. The following two tests are examples of several alternatives found in literature to the test introduced in this work, all of which require unnecessarily complex modeling or fabrication processes, involve expensive test setups, or provide results that are difficult to validate [8]–[13].

LDV MEASUREMENT OF ROUND PATCH DEFORMATION

Ababneh et al. present a test which involves actuation of a round patch of piezoelectric material and measuring the deflection profile near the edge of the patch using a laser doppler vibrometer. This test, while simple to fabricate, is extremely sensitive to LDV alignment and spot size. Automated spot alignment is an expensive feature for an LDV system and was not available at the time the test was needed [14].

FORCED CANTILEVER

Dubois and Muralt present an approach involving application of a force on a piezoelectric cantilever beam and measurement of the output charge. While the setup and fabrication steps are not complicated, the test requires that the user construct a perfectly fixed boundary condition relative to the beam or account for imperfections. The strain profile of a cantilever relative to tip deflection is extremely sensitive to the stiffness of the boundary condition, so this method is difficult to verify without known samples and is likely to be inaccurate [15].

II. ALN TEST SUMMARY

For this test, simple cantilever beam actuators are fabricated as described in the fabrication process section. Each beam is made of silicon with a thin layer of the AlN to be tested sandwiched between thin metal layers deposited on top as shown in the layer stack schematic in figure 3. An XY plane (top down) schematic of the standard actuator including the top metal layer pattern is shown in figure 4. While the bottom metal layer covers the full area of the device, the top layer is patterned as delineated in red. Beam parameters represented in these figures are described in table 2.

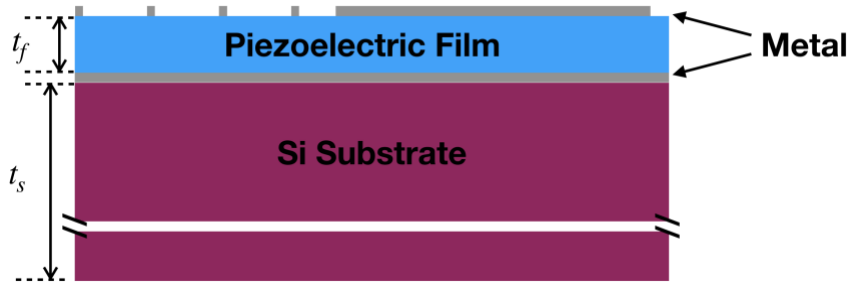

Figure 3: Layer-stack schematic of test device

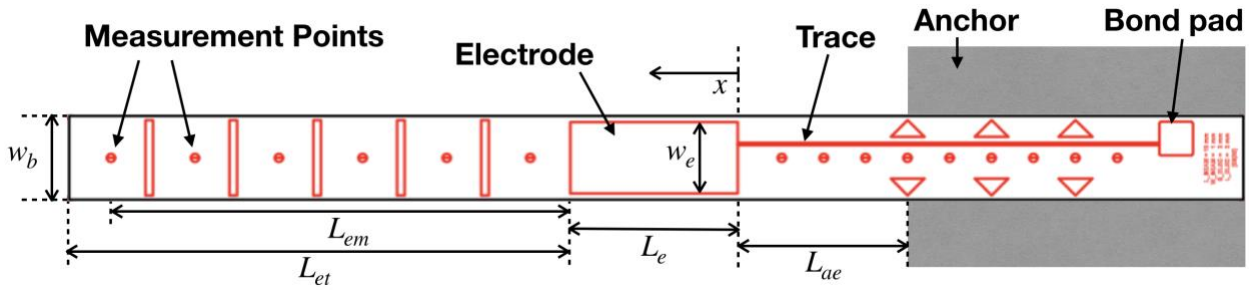

Figure 4: Top-down schematic of mounted test device

Parameter	Description	Value
L_{ae}	Distance from anchor to electrode	2mm (4mm)
L_e	Length of electrode	2mm
L_{em}	Distance from end of electrode to measurement point	5.5mm (3.5mm)
L_{et}	Distance from end of electrode to beam tip	6mm (4mm)
w_e	Width of electrode	.85mm
w_b	Width of beam	1mm
t_f	Thickness of piezoelectric film	~800nm
t_s	Thickness of substrate	520µm<t_s<560 µm

Table 2: Parameters specifying device geometry. Tabulated values are default simulation values and values used in primary test devices. When different from primary device parameters, values in parentheses describe the secondary test device used for test verification. 550 µm was used as the default simulation value for t_s.

For each device, the bottom electrode layer coats the full area of the device, while the top electrode layer is patterned. The pattern includes a bond pad, a rectangular patch for actuation of the piezoelectric material, and a trace connecting the two. Several small dots and lines of metal are also patterned, spaced at even intervals, which to not affect actuation but are used for alignment during measurement. Similarly, evenly spaced triangle shapes are patterned to indicate mounting positions. The AlN is etched away in one location to provide access to the bottom electrode layer, acting as a second bond pad for wiring the bottom electrode layer. These actuators are mounted by gluing the bottom of the beam area extending between a selected pair of triangles and the nearest end of the beam to a steel block. This block serves as an approximately fixed end for the cantilever. The bond pads are wired to an AC voltage source and impedance measurement system, and the impedance of the actuators is verified against calculated values. Then, the actuators are driven with a known AC voltage at far below resonance frequency, yielding

a Z displacement of the free end of the beam while exerting very little force on the fixed end. The displacement of each measurement point is determined using a laser doppler vibrometer and compared to simulations to determine piezoelectric constants. The fully assembled test setup is shown in figure 5.

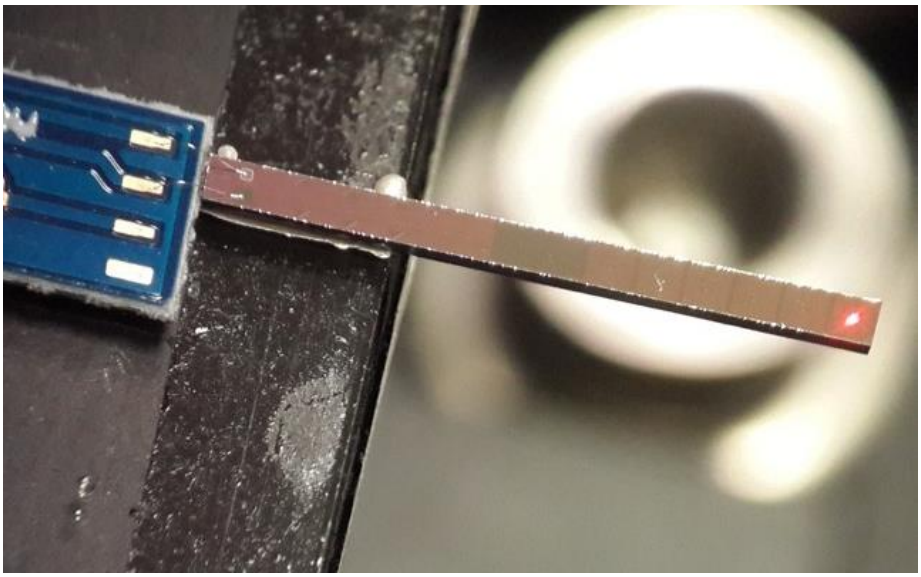

Figure 5: Mounted and wired test device during testing. The red LDV laser spot indicating the measurement point is visible .5 mm from the end of the beam.

In general, previously proposed tests accept complications because test and model boundary conditions are difficult to characterize. Silicon is very stiff, so designing fixed boundary conditions for silicon devices is extremely difficult. Furthermore, because piezoelectric films are often very thin compared to the substrate on which they are deposited, small changes in substrate properties or dimensions can have a significant effect on results of poorly designed tests. The described test overcomes these issues by measuring deflection of a simple piezo-actuated system within well-defined boundary conditions. The very low piezoelectric coefficients of AlN are particularly difficult to measure since bulk strain of AlN under normal operating voltages is near or below the

noise floor of many common measurement techniques. The measured deflection of the described system amplifies film strain enough for characterization of films with weak piezoelectric coupling. Furthermore, each test requires only a small area of a silicon wafer, common MEMS characterization equipment, and a very basic fabrication process that is compatible with many piezo-MEMS fab processes.

III. ANALYTICAL AND FEA MODELS

a. Static analytical model derivation

A static analytical model for device deflection was developed to validate numerical simulation results. This model is derived as follows:

By assuming uniform biaxial stress in a thin layer on top of a substrate, the effective transverse isotropic thin film piezoelectric constant $e_{31,f}$ is [16]:

$$e_{31,f} \equiv \frac{T}{E} = \frac{d_{31}}{s_{11}^E + s_{12}^E} \tag{5}$$

The film stress is calculated assuming uniform electric field and film:

$$T = \frac{d_{31} V}{\left(s_{11}^E + s_{12}^E\right) t_f} \tag{6}$$

Deflection can be calculated from film stress using the Stoney stress/deformation relationship for biaxial deformation of a plate [17]. This assumes uniform biaxial curvature, which is a good assumption for a thin, uniform cantilever beam when $t_f << t_s$. $R_{e,b} = \frac{w_e}{w_b}$ is a correction factor which is applied assuming a linear relationship between deflection and electrode width, which holds for R_{eb} close to 1 [18].

$$\delta = \frac{3(1-\upsilon_s) T t_f R_{e,b} x^2}{Y_s t_s^2} \tag{7}$$

Since 0 curvature and slope at the boundary is assumed, the slope of the actuated portion can be calculated from this formula by taking the derivative and applying (6). Since electric field, and therefore stress, only occurs in the actuated portion of the beam, the slope at the end of the actuated portion can be calculated by setting $x=L_e$, yielding:

$$\frac{d\delta}{dx} = \frac{6(1-\upsilon_s) R_{e,b} L_e d_{31} V}{Y_s t_s^2 (s_{11}^E + s_{12}^E)} \tag{8}$$

Since there are no other stresses, the slope remains constant between the end of the electrode and the end of the beam, yielding the following function for beam displacement beyond the end of the electrode

$$\delta = \frac{3(1-\upsilon_s) R_{e,b} d_{31} V}{Y_s t_s^2 (s_{11}^E + s_{12}^E)} \left(L_e^2 + 2L_e(x - L_e)\right) \tag{9}$$

As calculated, the ideal beam exhibits the static deflection shape shown in figure 6.

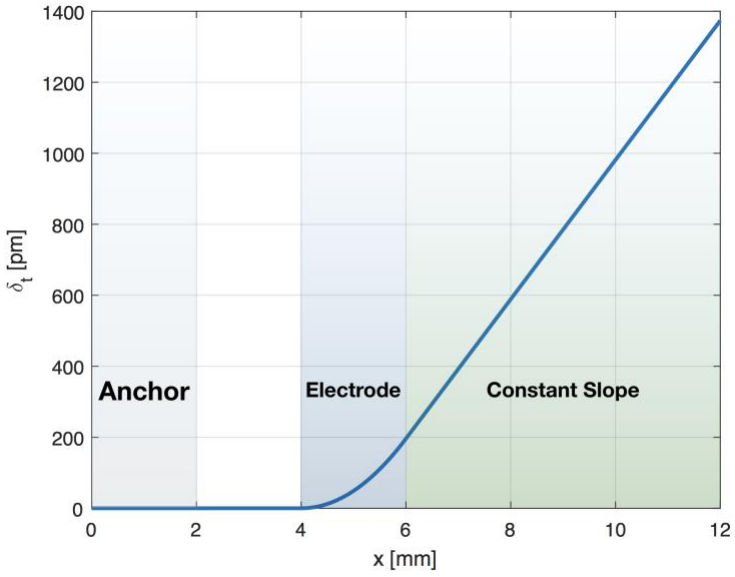

Figure 6: Deflection profile vs. location along the beam for the default measurement device simulated using the analytical model. The anchored region, the electrode region, and the constant slope region are labeled in gray blue and green respectively. Note that x in this plot does not match x in (7)-(9), since these equations assume that x=0 at the anchor side of the electrode region.

As shown, no curvature occurs at the fixed end of the beam, so theoretically no stress is applied at the boundary. This relaxes the requirement that the anchor must be extremely stiff, circumventing the practical issues associated with constructing an extremely rigid fixture.

The analytical model also reveals useful information about the sensitivity of results to design parameter variation. For instance, the measured deflection is inversely proportional to the thickness of the beam squared. Because of this, accurate measurement and simulation of the thickness of the beam is critical. The model also shows that as long as the piezoelectric film is very thin relative to the rest of the beam (assumed when using the effective piezoelectric coefficient, $e_{31,f}$), the thickness of the AlN film only effects the

deflection of the beam by changing the stiffness and thickness of the overall structure. Since the film's thickness is much smaller than the overall thickness, this effect is negligible. For this reason, measurement and accurate simulation of film thickness is only important when the film is of stiffness or thickness comparable to the rest of the beam.

b. Numerical model

VALIDATION VS. ANALYTICAL

The analytical model was not used to calculate d_{31} for tested films. Because the analytical model only applies for nearly uniform biaxial stress, the thin electrode trace necessary for connecting the actuated patch to the bond pad cannot be accurately represented. Only the electric field at the actuated patch is modeled, but an electric field is also applied to the piezoelectric material beneath the trace, increasing the overall deflection of the beam. A Finite Element model of the cantilever beam was developed in ANSYS Mechanical APDL to account for inaccuracies in the analytical model. Comparing the analytical and numerical models also provided a means of validating of the test in the absence of explicit experimental validation, which would require obtaining films with known piezoelectric properties. Acquiring known samples was deemed too expensive and unnecessary. Further opportunities for validation of the two models are discussed in the experimental results/discussion section (6C). The numerical model was also used to study the dynamic response of the beam.

When comparing a simulation to measurements, accurate material properties for both the numerical simulation and the analytical model are crucial. Because the beam's x-axis was oriented along the silicon wafer's (110) direction, the stiffness matrix for silicon was selected to match this orientation. Properties assuming an orientation that is rotated by 45 degrees are often mistakenly used for silicon because these are the most commonly reported values in literature. Simulations using an incorrectly rotated stiffness tensor yielded deflection results up to 10% lower. Silicon wafer stiffnesses are well-controlled, so reported values were deemed acceptable [19].

First, static numerical simulations were conducted without accounting for the trace to verify agreement with the analytical model. Numerically simulated beam tip deflection applying default parameters was 1371 pm, compared to 1373 pm for the analytical model, yielding less than .2% error for this case. Default beam parameters matching the actual beams fabricated for this work are shown in table 2. Sensitivities are tested by varying a single parameter from the default set at a time. Results of simulations demonstrating the effects of various beam parameters on low frequency beam tip deflection were compared to sensitivities predicted by the analytical model. Results are plotted in figure 7. This demonstrates agreement between the two models when traces are not included.

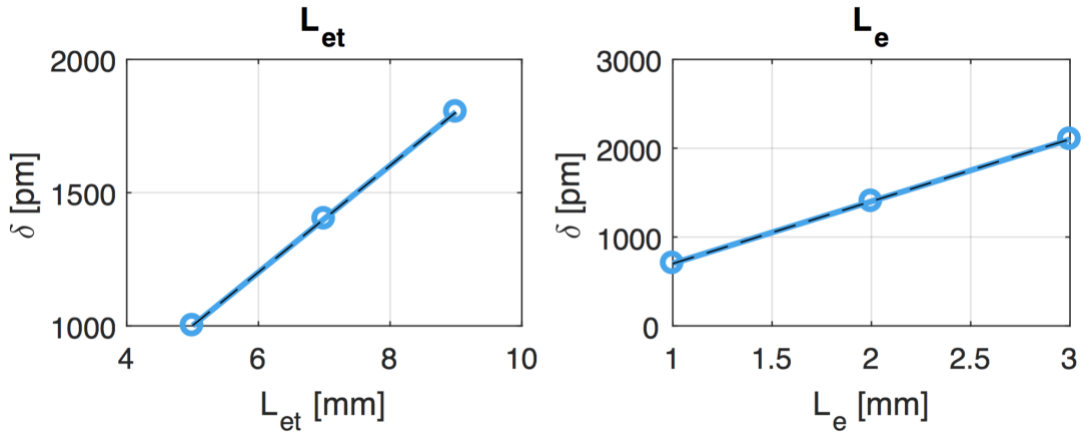

Figure 7: Beam tip deflection results of numerically simulated test devices (blue lines) plotted alongside predicted sensitivities (dashed lines), varying each test device parameter from the default set of parameter values individually. Predicted sensitivity lines are calculated by starting with the tip displacement of a beam with default parameters (δ = 1401.5 pm) and calculating the variation from this tip deflection value based on the predicted sensitivity of tip deflection to the given parameter as determined by the analytical model.

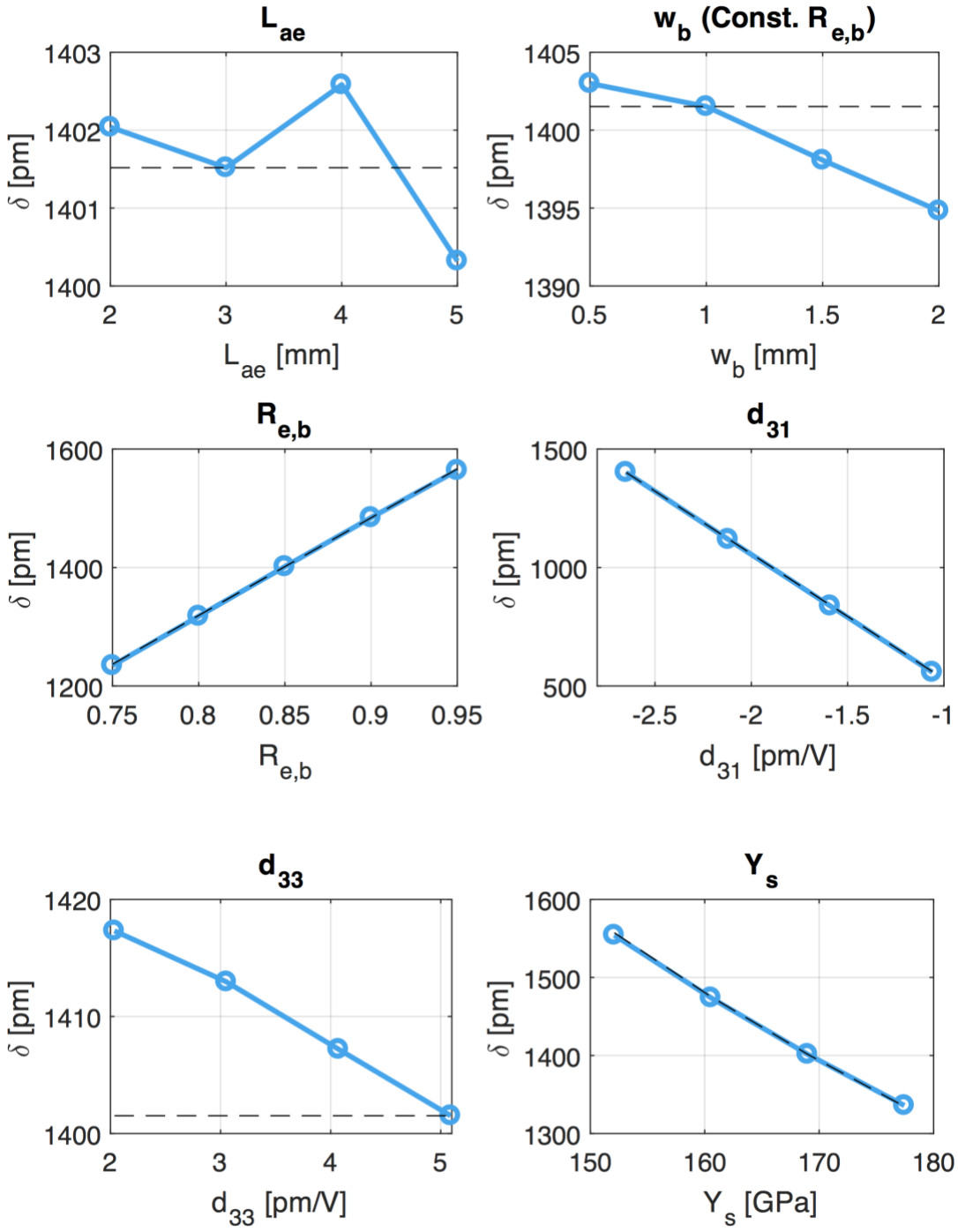

Figure 7: (cont.)

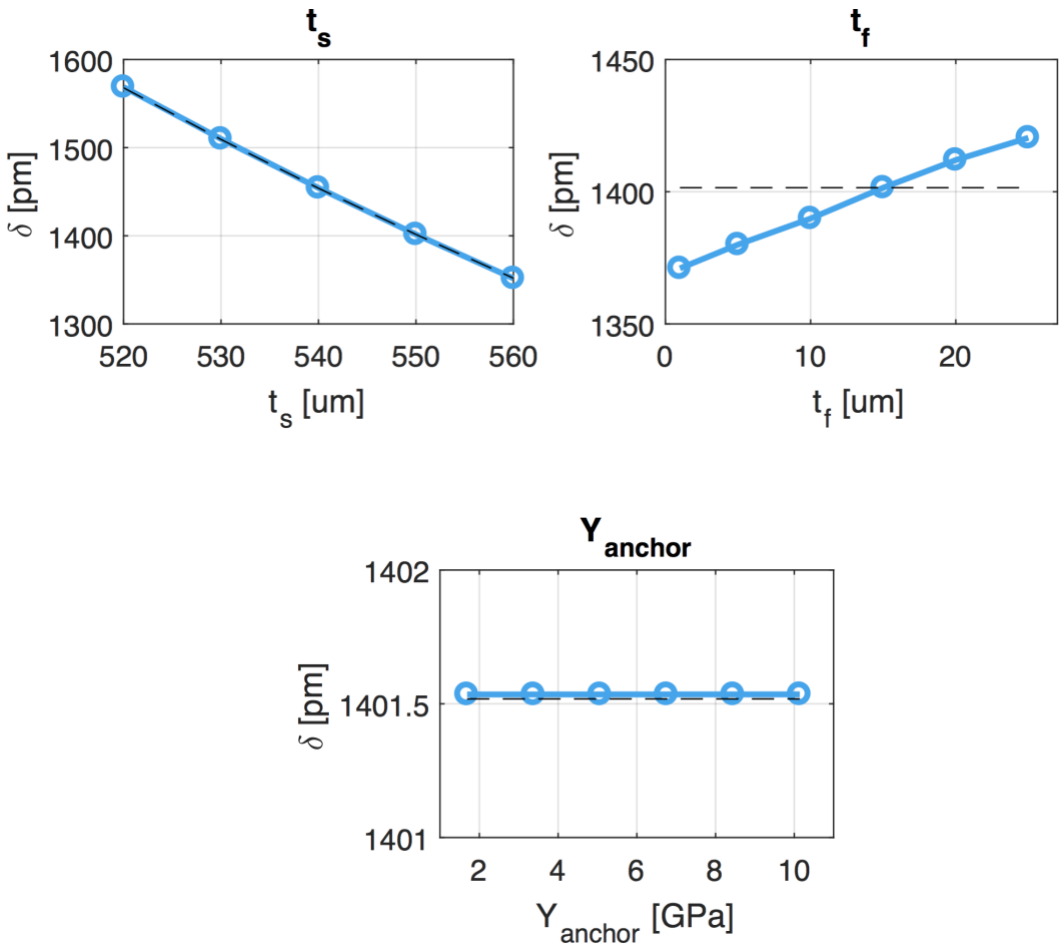

Figure 7: (cont.)

Because thin films require a very fine simulation mesh, sensitivity test simulations were conducted using a default t_f =15 µm. All values in the film's CE matrix are multiplied by 1/15 to yield equal stiffness to a 1 µm thick film. Effective piezoelectric coupling is conserved by specifying the *e* matrix instead of the *d* matrix. The increase in overall beam thickness increases the bending moment applied by the film, and subsequently the deflection, yielding a systematic ~3% increase in deflection as compared to 1µm thick AlN (figure 7, t_f), but the change facilitates much faster and

simpler simulations. A 1 μm thick film is modeled when calculating d_{31} values during testing, eliminating this error.

RESONANCE FREQUENCY PREDICTION

The equation for the natural frequency of an ideal cantilever beam is:

$$f_{res} = \frac{1.875^2}{2\pi}\sqrt{\frac{Yt^2}{12\rho L^4}} \tag{10}$$

Using beam parameters as listed in table 2 and $2328\,\frac{kg}{m^3}$ for the density of silicon, this yields a resonant frequency f_{res}=7.569 kHz. However, the ideal cantilever beam model is not valid because test beam resonance frequencies are drastically affected by the stiffness of the imperfect fixed end of the cantilever. Cantilevers fixed using layers of adhesive with varying compliance were simulated. Resulting calculated fundamental resonance frequencies are plotted vs. adhesive stiffness in figure 8. Because of significant variation in bond stiffness for a given adhesive, model-based prediction of resonance frequency for a real beam is difficult.

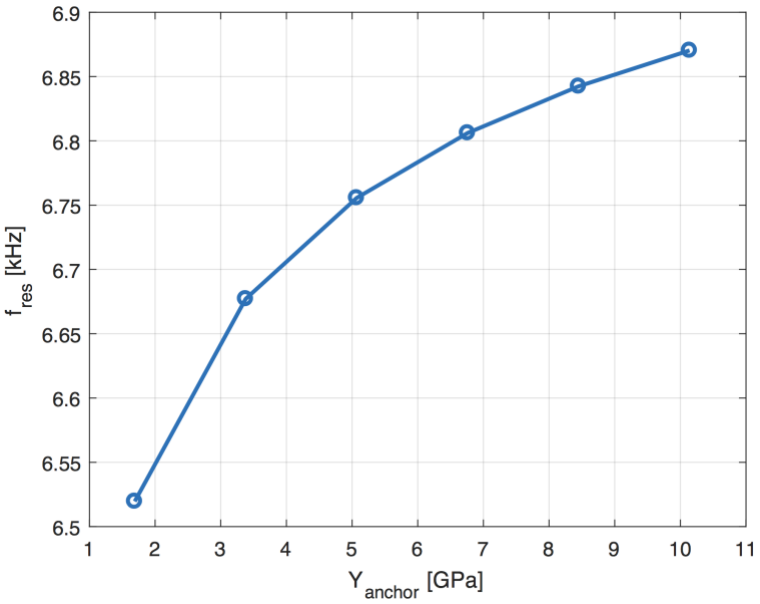

Figure 8: Simulated test beam fundamental resonance frequency vs. anchor of stiffness Y_{anchor} where the anchor is a 50 µm thick layer of simulated adhesive fixing the beam's anchor region to a rigid boundary.

DYNAMIC RESPONSE SIMULATION

Because of frequency dependent effects of beam inertia and damping relative to beam stiffness, a cantilever beam's deflection profile is frequency dependent. However, far below the fundamental resonance frequency, the mechanical impedances associated with beam inertia and damping are small compared to the impedance associated with beam stiffness. Because of this, deflection due to low frequency actuation converges to the same profile as the static case even at non-zero actuation frequencies. When inertia and damping are significant, forces are exerted along the entire length of the beam, including at the "fixed" end. Because this boundary condition is not truly fixed, any forces exerted here cause deflections that cannot be modeled effectively without knowing the exact stiffness of the fixture, invalidating the test. Therefore, frequency dependence or even small deviation from the static deflection shape yields an invalid test. Simulated deflection profiles of the top of a measured beam assuming an unrealistically stiff anchor (Y_{anchor}=13 TPa) are shown at various actuation frequencies in figures 9 and 10. The

zoomed plot in figure 10 clearly shows the increase in curvature at the anchor as frequency increases, indicating an increase in force exerted on the anchor. Despite the extremely stiff anchor, some deflection still occurs at the anchor at high frequencies.

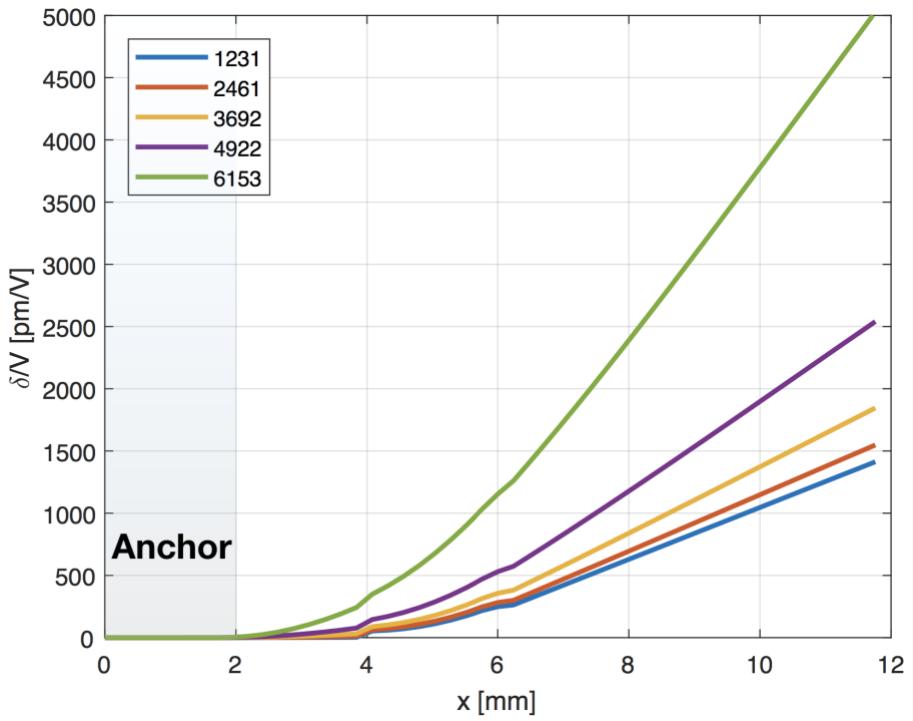

Figure 9: Deflection profiles vs. location along the beam for default measurement devices simulated using the numerical model for various actuation frequencies (in Hz). An extremely stiff, but not perfect 100 µm thick layer of simulated adhesive (Y=13 TPa) is used to fix the plate. The length of the beam fixed to the anchor is highlighted in gray. Deflection at the anchor increases vs. actuation frequency.

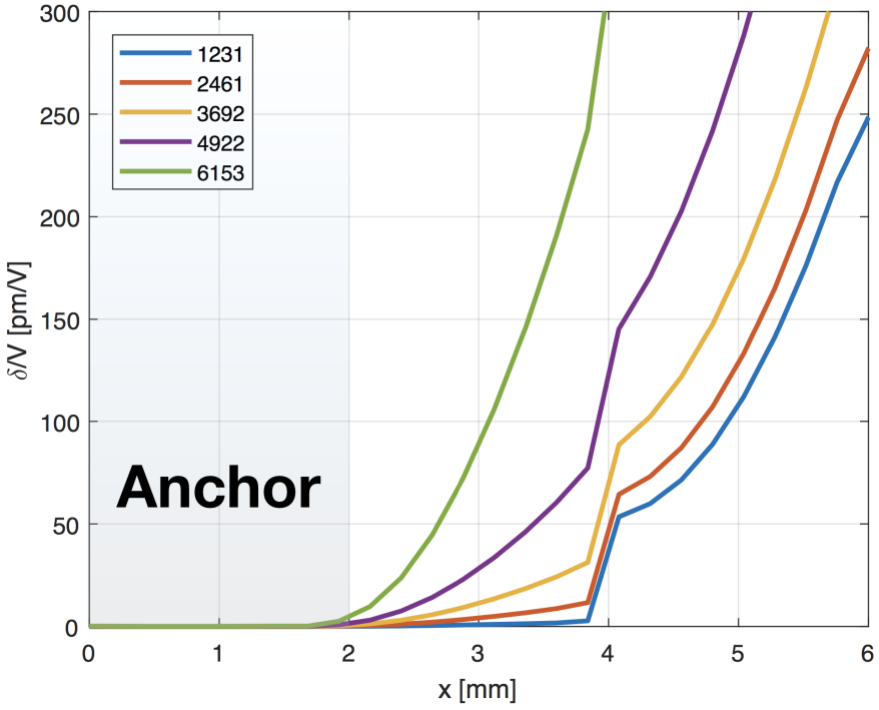

Figure 10: Same plot as figure 9 zoomed in to show detail. Deflection of the anchor occurs at high frequencies despite an unrealistically stiff constraint.

IV. EXPERIMENTAL SETUP

a. Device layout.

Two test devices were designed for the experiment, a primary device, and a secondary device for verifying results of the primary device. Secondary device is identical to the primary device except for the location of the electrode, which is shifted 2 mm further from the anchor. These values are listed above in table 2.

b. Fabrication process

The test device fabrication process is relatively simple, requiring only 2 masks and only steps that are generally required in any AlN deposition. Mask layouts are shown in figures 11 and 12 as drawn. Red lines indicate Mask 1, while green lines indicate Mask 2. Yellow lines indicate dicing paths. Masks also included round electrode patches, which were used for a separate test considered before the development of the test discussed in this work.

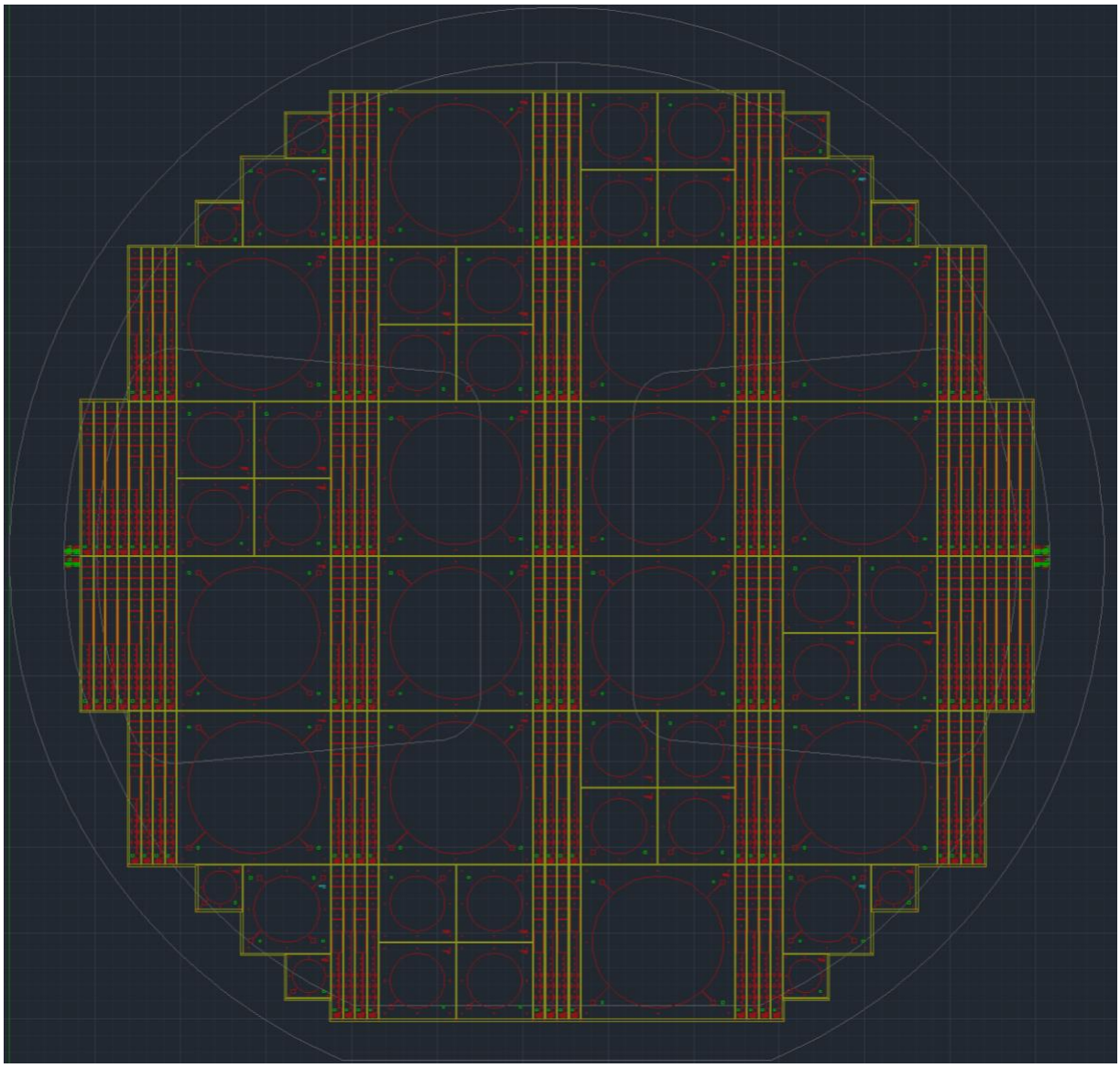

Figure 11: Mask layout for full wafer showing beam devices and circular patch devices from a separate material test attempted previously [14]. Red lines indicate Mask 1, while green lines indicate Mask 2. Yellow lines indicate dicing paths.

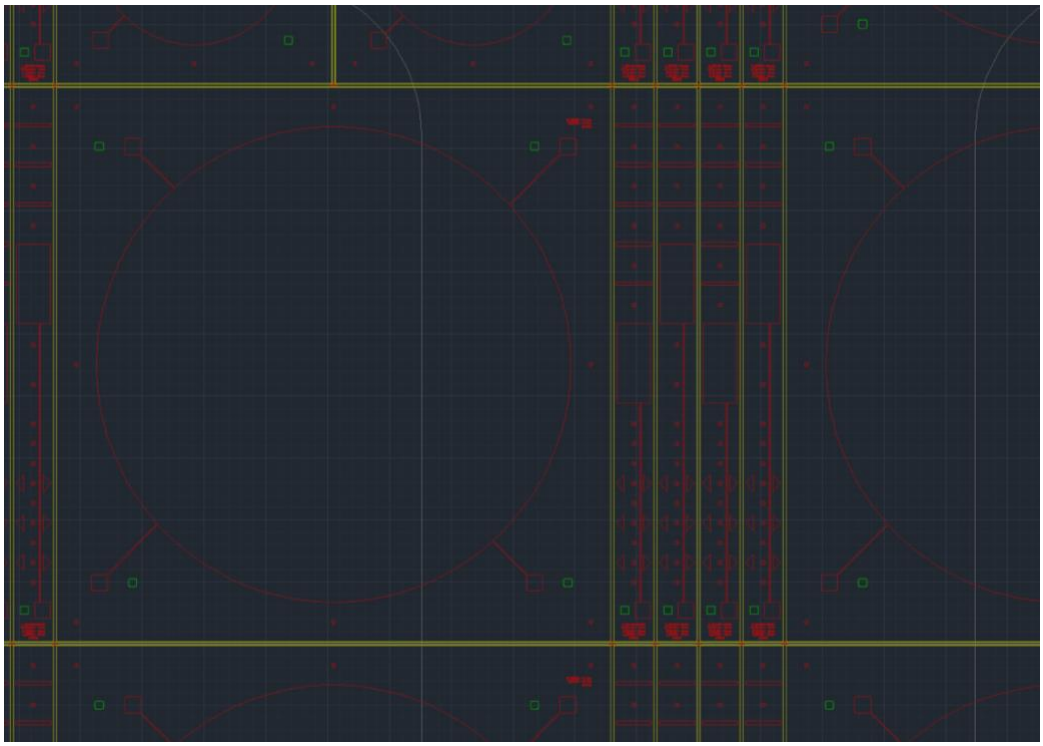

Figure 12: Zoomed-in image of mask layouts showing more detail

As shown, each fabricated wafer produced a maximum of 120 devices.

FABRICATION PROCESS

The general fabrication process used for each wafer is as follows:

1. A ~500 µm thick Si wafer is cleaned.
2. A 300 nm thick SiO2 layer is grown on the wafer in an MRL furnace.
3. A Pt electrode layer is sputter deposited onto the wafer. When a Ti layer is included, the Pt is followed immediately by a Ti layer sputter deposition. This forms a ~130 nm thick bottom electrode, which serves as a seed layer for the AlN.
4. The surface of the electrode is solvent-cleaned, and AlN is sputter-deposited using the deposition process parameters under test.

5. Mask 1 is used to pattern AZ9260 photoresist onto wafer for top electrode pattern. A second Pt/Ti electrode is deposited using the same process described above.
6. Lift-off removes metal on top of patterned photoresist, leaving a patterned top electrode.
7. Mask 2 is used to pattern photoresist for the AlN etch process.
8. AlN is acid etched using this pattern to provide access to bottom electrode.
9. The wafer is then diced into rectangles, yielding devices like the one shown in figure 5.

c. Pre-test thickness and admittance measurements

Because device thickness has a significant impact on deflection results, device thickness was measured using a scanning electron microscope and recorded for use as simulation parameter input. The film thickness was also measured to allow for capacitance estimation to verify the dielectric constant.

Before mounting, the input admittance of each beam was measured. The film and a resistor of resistance R=10 kΩ, with both ends of the circuit grounded. A known AC input voltage (V_{in}) at f=10000 kHz is then applied across the resistor. The capacitance of a device was then calculated by measuring the voltage across the film (V_{out}) and using the following equation:

$$C=\frac{1}{(2\pi fR)}\frac{V_{out}}{V_{in}} \tag{11}$$

The capacitance was also predicted using the equation:

$$C=\frac{\varepsilon_{33}\varepsilon_0 A}{t_f} \tag{12}$$

where A is the total area of the electrode, trace, and bondpad. Because the loss tangent of AlN is extremely small, device impedance should be primarily capacitive, especially at high frequency, so series resistance can be safely ignored. Devices generally exhibited capacitances within 2% of the predicted value, and error larger than this was generally an indicator of a defective device. This test was also conducted at DC to verify that DC

impedance is high. Beams with a low DC impedance were deemed defective and removed from the experiment.

d. Deflection measurement process

The beams were then mounted by fixing a portion of the bottom of the beam to a steel block using adhesive and wired out as shown previously in figure 5. Cyanoacrylate adhesive was selected for its ease of use, acceptably low viscosity, and high stiffness.

DISPLACEMENT DETERMINATION

Displacement measurements were taken using a Polytec PDV100 laser doppler vibrometer. For each measurement, the vibrometer spot was aligned and focused on the desired measurement location, demarcated by one of the circular dots included in the top electrode pattern. The beam was then actuated at ~9V, which was deemed the highest AC voltage that could be applied without risk of damaging the approximately 800nm film at the selected actuation frequency. The LDV output of the displacement of the beam at the selected actuation frequency was recorded for each point measured.

FREQUENCY SELECTION/ENSURING PROPER DEFLECTION SHAPE

First, in order to verify the deflection shape and select an actuation frequency, measurements were taken at all demarcated measurement points. To select an actuation frequency, test beams were measured at several actuation frequencies, selecting the highest frequency at which displacement results were not frequency dependent. As discussed later in section 6b, the beam is likely to exhibit a profile very similar to the characteristic static deflection profile shown in figure 6 even at invalid frequencies. Slight curvature due to inertia can significantly alter tip-deflection measurements, so simply checking for linearity does not necessarily validate an actuation frequency. Valid frequencies tend to be around 1/10 of the calculated ideal fixed-end cantilever resonance frequency depending on beam dimensions and damping.

e. Calculation of d_{31}

Only one measurement at a single point is necessary to determine d_{31} for the beam, so beams were measured only at the point furthest from the anchor once a safe actuation frequency was selected. This was the primary measurement point because it is expected to exhibit the highest expected displacement on the beam, providing the highest SNR.

The piezoelectric coefficient d_{31} was calculated from these measurements by comparing the measurement point deflection to the deflection of a matching simulated beam. As discussed previously, displacement at a given point is proportional to d_{31}, so measured d_{31} was calculated using the following equation:

$$d_{31} = \frac{\delta_{measured}}{\delta_{simulated}} d_{31,ideal} \tag{13}$$

Other piezoelectric coefficients can be determined from d_{31} when stiffness, dielectric permittivity, and Poisson's ratio are known. Large variations in these three properties are uncommon from film to film, so reported values are often a reasonable assumption for estimating all other piezoelectric coefficients once one coefficient is determined.

f. Test design details

LDV NOISE FLOOR

The velocity noise floor of the PDV100 LDV is $20 \frac{\text{nm}}{\text{s}} / \sqrt{\text{Hz}}$ [20] under optimal conditions. Because LDVs measure velocity, this translates to a frequency-dependent displacement noise floor of $f \times 40\pi \text{ nm} / \sqrt{\text{Hz}}$. For this reason, beams were actuated at as high a frequency as possible without deviating from the static displacement profile. Increasing resonance frequency by reducing the distance between the anchor and the electrode or by stiffening the boundary condition does not reduce deflection, but increases the maximum actuation velocity, improving test precision. In practice, the LDV

noise is not the limiting factor in test precision, except when the actuation frequency or measured coupling coefficient is low, or when very small test devices are measured.

VARIABLE PIEZOELECTRIC CONSTANTS VS. LOCATION: YIELD CONSIDERATIONS

Maximizing device yield is particularly important because the quality of an AlN film is variable with respect to location on a wafer. When a device is defective, the film quality in that location cannot be determined.

The total area of the electrode patch determines the area of piezoelectric material that is driven by the applied voltage. Considering previous discussions, it seems beneficial to increase the size of this patch in order to yield maximum displacement of the measurement points, increasing SNR. However, small defects are often present even in otherwise high quality AlN films. As the actuated area increases, the likelihood of a defect occurring within this area increases. Because the actuated area of this test device is much larger than common piezo-MEMS devices, the probability of a defect occurring in this area is relatively high. The area of the patch was limited to reduce this probability, increasing device yield.

ELECTRODE PATCH LOCATION

Beams are designed with a small distance between the fixed end and the electrode patch to ensure that these areas do not overlap, causing the stiffness of the boundary condition, which cannot be affectively simulated, to affect displacement. Displacement should be measured at a point between the electrode patch and the anchor to verify that this region remains motionless, indicating a successful fixed boundary condition at the selected actuation frequency.

BOUNDARY CONDITION SELECTION

As discussed earlier, structural boundary conditions of most test structures for piezoelectric properties are difficult to characterize or control. Many methods for fixing

the end of a cantilever beam are available, but in practice all fail to act as perfectly rigid conditions in many cases. While the test was designed to minimize force at the boundary condition, the maximum allowable actuation frequency depends on the stiffness of the cantilever system, which is significantly reduced by a compliant fixed end. Two primary options for fixing the end of a beam were considered: clamping, and gluing.

Clamping a beam between two stiff surfaces is a fast, simple method for building a fixed condition. However, this method was determined to be impractical. Applying a clamping force to a very delicate beam risks cracking or destroying the beam before a measurement can be made. Applying a clamping force to both the top and bottom of the beam also restricts access to the fixed portion of the beam, and wired bond-pads placed on a non-fixed portion of the beam would affect beam dynamics. Pads could also be placed in an area of the fixed portion not covered by the clamp. This would either require a specially designed clamp to avoid covering the entire top of the fixed portion of the beam, which is costly and could sacrifice clamp stiffness, or would require an extremely long fixed portion, wasting wafer space.

Instead, adhesive was used to fix the beam to a rigid block. While this does not provide as rigid a boundary condition as clamping, adhesive does not restrict access to the top of the beam and is less likely to destroy beams. Cyanoacrylate adhesive was selected for short application and curing time, low viscosity, and high stiffness.

V. EXPERIMENTAL RESULTS/DISCUSSION

Example simulation output, measurement data, and calculated d_{31}values are presented for various cases. An acceptable actuation frequency is determined, beam designs with different actuated portion locations are compared, and measured d_{31} values are compared alongside their corresponding XRD measurement results.

a. Numerical model results

The numerical model was used to simulate two beam designs that were tested. Example results are shown in table 3. These results were compared to measurement data collected as described in section 5d in order to determine measured d_{31} values.

		T_si		
		530 µm	**540 µm**	**550 µm**
Beam	**Primary**	1493	1438	1387
	Secondary	1118	1077	1039

Table 3: Simulated deflection values ($\delta_{simulated}$) at the furthest measurement point from the anchor for primary (L_{ae} = 2 mm) and secondary (L_{ae} = 4 mm) beams resulting from numerical simulations including traces and 1 µm piezoelectric film for comparison to measured data. Using this data, measured deflections, and (13), measured d_{31} values can be calculated.

b. Actuation frequency selection

Deflection profiles are measured with actuation frequencies of 700 Hz and 1500 Hz at all measurement points and plotted in figure 13. Separate linear regressions are calculated from measurements at points 1 through 6 for 700 Hz and 1500 Hz, yielding high r^2 values (.999993 and .999945 respectively), which indicate excellent linearity. Even so, the percent difference between primary tip deflections at these two frequencies is 3.7%. While this error is not large, this difference indicates that simply checking for linearity is not a safe method for determining a valid actuation frequency. Deviation from this regression is plotted in figure 14, presenting clear curvature which hints at the presence of resonance effects at 1500 Hz. Small errors or noise in measurements are

likely to obfuscate this shape, so it is difficult to verify from this data whether or not actuating at 700 Hz provides a valid measurement.

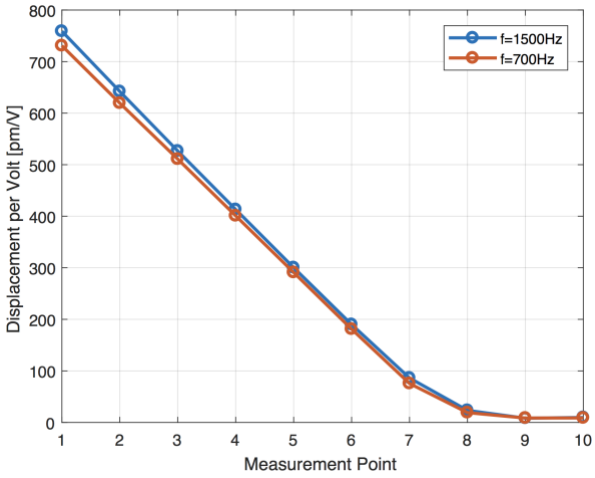

Figure 13: Measured beam deflection profiles vs frequency as measured at demarcated measurement points. Measurement point 1 is closest to the end of the beam.

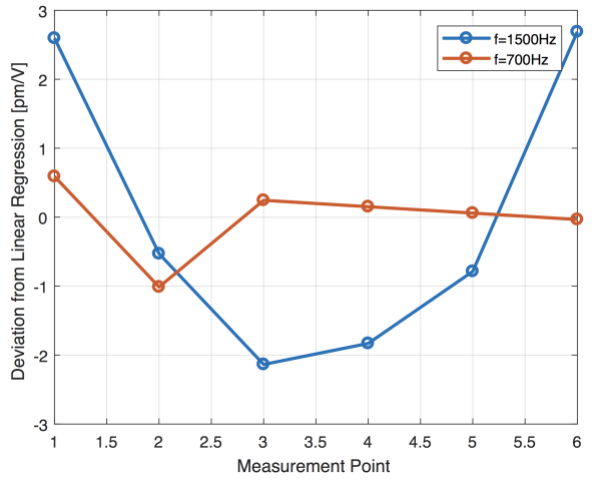

Figure 14: Deviation of deflection at each measurement point from a linear best-fit line calculated for data from measurement points 1 through 6.

Instead, a simple displacement convergence test is conducted. The results are listed in table 4 and plotted in figure 15. The measured displacement converges on 730 pm/V at ~700 Hz. % difference is less than .3% compared to 500 Hz and 300 Hz, confirming that 700 Hz is a valid actuation frequency.

Frequency	δ **[pm/V]**
1500	758.56
1002	739.58
697	730.79
498	729.26
298	730.89

Table 4: Measurement point deflection results vs. frequency for example test device (wafer a)

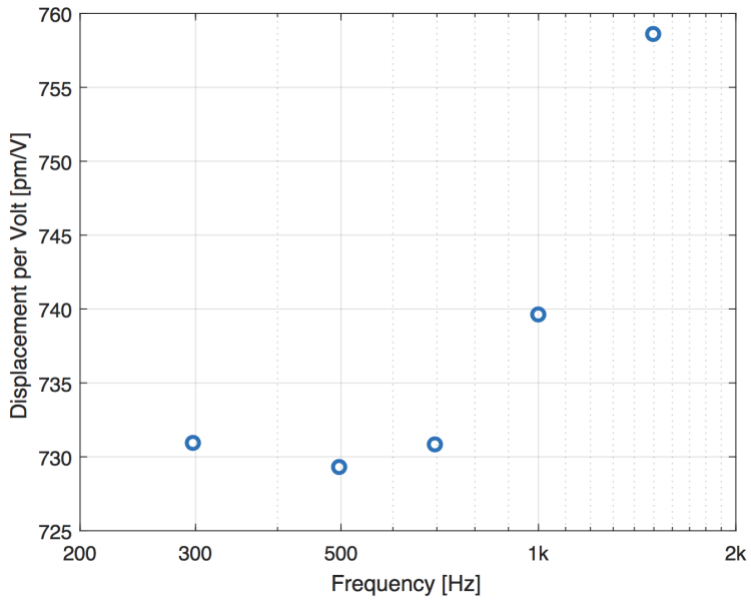

Figure 15: Measured displacement at measurement point 1 vs. frequency showing convergence on 730 pm/V at 700 Hz

As calculated using (13), d_{31}= -1.43 pC/N for this device, only 54% of the reported value, indicating a low quality film.

c. Repeatability for varying beam designs

Measurement data for beams from adjacent locations on a wafer is presented for two different wafers in table 5. Because piezoelectric film quality tends to vary gradually across a wafer, beams from adjacent positions on a single wafer are predicted to have the most similar d_{31} values, though values cannot be assumed to be identical. In calculations using the numerical simulation, differences between the calculated d_{31} values on each wafer are within reasonable variation between devices. Using the analytical solution yields significant differences in results between adjacent devices as shown in table 6. This provides evidence that traces are well accounted for in numerical simulations.

Wafer	**Beam Design**	**t_{si} [um]**	**δ/V [pm/V]**	**Measured d_{31} [pC/N]**	**$d_{31}/d_{31,theory}$ [%]**
a	Primary	550	731	-1.43	54.1
a	Secondary	550	538	-1.41	53.6
e	Primary	530	1274	-2.32	87.5
e	Secondary	530	944	-2.30	87.1

Table 5: Measured thickness, deflection, and corresponding d_{31} values calculated using $d_{31,theory}$ results from the complete numerical model for beams using primary and secondary beam designs for two example wafers. Deflection values were taken from the beam exhibiting the maximum deflection result among several tested beams from each wafer.

Wafer	**Beam Design**	**t_{si} [um]**	**δ/V [pm/V]**	**Measured d_{31} [pC/N] (Analytical model)**	**$d_{31}/d_{31,theory}$ [%] (Analytical)**
a	Primary	550	731	-1.52	57.3
a	Secondary	550	538	-1.61	60.9
e	Primary	530	1274	-2.46	92.7
e	Secondary	530	944	-2.63	99.3

Table 6: Measured thickness, deflection, and corresponding d_{31} values calculated using $d_{31,theory}$ results from the analytical model for beams using primary and secondary beam designs from two example wafers. Deflection values were taken from the beam exhibiting the maximum deflection result among several tested beams from each wafer.

d. Example use-case: AlN deposition troubleshooting

The AlN test was designed specifically for facilitating the development of an AlN deposition process in the Microelectronics Research Center at The University of Texas at Austin. The objective was to achieve films with piezoelectric coefficients (e.g. d_{31}) that were at least 75% of the reported value for optimized AlN. The device fabrication process is summarized in section 5a. All wafer fabrications were conducted or overseen by Yoonho Seo. Specific parameters of the sputtering process were the subject of experiments involving fabrication of roughly 40 wafers. Experimental parameters were selected after a review of literature on the subject of plasma sputtering [1], [6], [7], [11], [14], [21]–[26]. Most attempts yielded shorted, cracked, or otherwise corrupted devices which did not require testing of piezoelectric coefficients. Once working devices were achieved, d_{31} values of fabricated wafers were tested and improved until the target was reached. N_2 gas flow rate and seed layer material were two parameters subjected to experiments after working devices were achieved.

Three wafers of devices were fabricated and tested using unique recommended flow rate values reported in literature while holding other parameters constant. 60 sccm N2 gas flow rate yielded the highest tested piezoelectric properties.

A similar experiment was then conducted comparing two seed layer compositions: a Pt/Ti stack (used previously), and Pt. Using the adjusted N2 gas flow rate, another wafer was fabricated using Pt as the seed layer. Using a Pt seed layer increased the measured coefficient by >25% of the theoretical value, surpassing the target piezoelectric coefficient.

A more rigorous DOE involving more parameter values and accounting for nonlinear interactions between parameters would certainly have yielded higher piezoelectric coefficients, but highly optimized film was unnecessary for developing functional AlN for prototyping. Two more wafers were fabricated and tested to verify the

stability of the process. Results of piezo coefficient tests for each wafer are shown in table 7.

Wafer	**N2 gas ratio (Ar/N2) [sccm]**	**Seed Layer Material**	**d31 ratio [%]**	**d31 [pC/N]**
b	80% (20/80)	Pt/Ti	56.4	1.49
c	83% (20/100)	Pt/Ti	43.2	1.15
d	75% (20/60)	Pt/Ti	60.0	1.59
e	75% (20/60)	Pt	87.5	2.28

Table 7: AlN deposition process parameters and corresponding maximum measured d_{31} values for several wafers fabricated during optimization of deposition process.

X-ray diffractometry measurement data for wafers c and d is shown in figure 16. Peaks indicating the presence of a particular crystal orientation are shown. Higher, sharper peaks indicate materials that are more uniformly aligned in that particular orientation. A 20x increase in FWHM (full-width half-maximum) of peaks corresponding to AlN is observed when switching from a Pt/Ti to a Pt electrode. This indicates significant improvement in AlN orientation, predicting much stronger piezoelectric coupling. This agrees with measured coefficients.

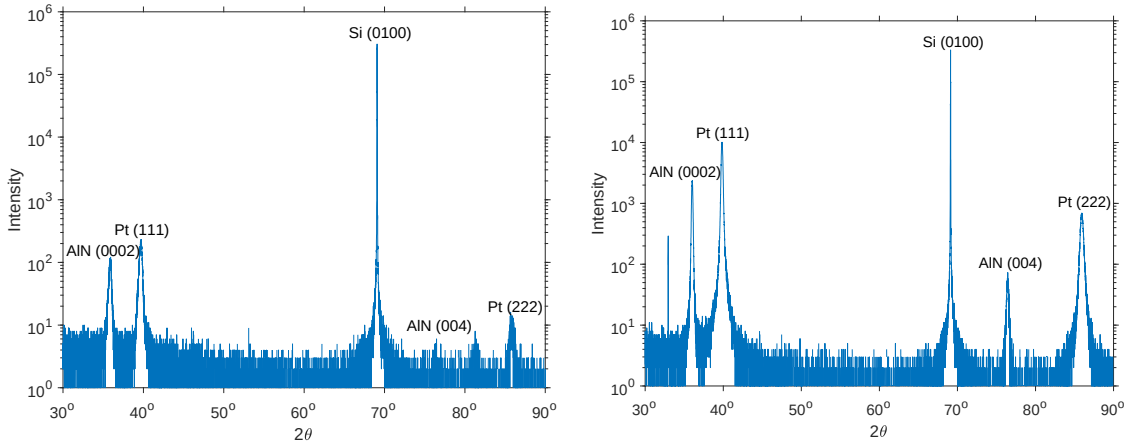

Figure 16: XRD measurements of wafers a (left) and e (right) showing significant increase in AlN (0002) peak intensity corresponding with increase in d_{31}. Measurements were taken at the center of each wafer.

VI. SOURCES OF ERROR/FURTHER STUDY

Because high precision wasn't necessary, wafer space was not a concern, and only linear properties were determined, necessary beam parameters were not optimized for maximum SNR, minimal size, or high bandwidth. Instead, they were designed to facilitate verification. Several simple parameters changes could be made to improve the performance of the test devices including moving the electrode closer to the anchor and increasing its length relative to the length of the beam. Numerical modeling could be applied to optimize beams for maximum SNR at a given size. This would be useful for optimizing fabrication of materials with low piezoelectric coefficients and for checking material properties during a device fabrication process when wafer space is costly. In these situations, SNR is likely a dominant source of error.

One notable source of error in the experiment was lack of precision when measuring device thickness t_{si}. This value was measured and recorded with a resolution of 10 nm, which is ~2% of the thickness of the device. A 2% thickness measurement error translates to approximately 4% error in modeled displacement and d_{31}, which was not deemed large enough error to necessitate a more precise measurement. For future tests that require more precision, this is an easily remedied major source of error.

While misalignment didn't yield significant issues with repeatability during the experiment, it is a potential source of error. Using a scanning LDV like the Polytec PSV-500 instead of manual alignment would facilitate accurate spot placement and speed up measurements. This is a much more expensive option [27].

Measurement of nonlinear material properties is also possible with these devices. Frequency and magnitude dependent nonlinearities are common for piezoelectric materials [28]. A nonlinear d_{31} value could be measured by actuating at several higher voltages and at several frequencies. The bandwidth of these tests could be increased without encountering resonance effects by increasing the stiffness of the cantilever system, including the fixed boundary, and by reducing damping.

VII. CONCLUSION

The piezoelectric coefficient test presented, though not experimentally verified, passes other tests including matching analytical vs. numerical models and checks for repeatability in spite of a parameter change. Test results also correlate well with XRD measurements, another indicator of film quality. The test was successfully used to develop an AlN deposition process yielding film with d_{31} = 2.28 [pC/N] which is 87.5% of the theoretical value, exceeding the author's target piezoelectric coefficient.

Works Cited

[1] K. Uchino, "Introduction to Piezoelectric Actuators and Transducers Kenji Uchino , International Center for Actuators and Transducers , Penn State University," no. 5, p. 40, 2003.

[2] S. Moheimani and A. Fleming, "Fundamentals of Piezoelectricity," in *Piezoelectric Transducers for Vibration Control and Damping*, London: Springer-Verlag, 2006, pp. 9–35.

[3] Y. Seo, D. Corona, and N. A. Hall, "On the theoretical maximum achievable signal-to-noise ratio (SNR) of piezoelectric microphones.," *Sens. Actuators. A. Phys.*, vol. 264, pp. 341–346, Sep. 2017.

[4] User:Soid_state, "GaN Wurtzite polyhedra.png - Wikimedia Commons," 2008. [Online]. Available: https://commons.wikimedia.org/wiki/File:GaN_Wurtzite_polyhedra.png#metadata. [Accessed: 26-Nov-2018].

[5] S. S. Gevorgian, A. K. Tagantsev, and A. K. Vorobiev, *Tuneable Film Bulk Acoustic Wave Resonators*. London: Springer London, 2013.

[6] I. Safi, "Recent aspects concerning DC reactive magnetron sputtering of thin films: a review," *Surf. Coatings Technol.*, vol. 127, no. 2, pp. 203–218, 2000.

[7] C. Stoeckel, C. Kaufmann, R. Hahn, R. Schulze, D. Billep, and T. Gessner, "Pulsed DC magnetron sputtered piezoelectric thin film aluminum nitride - Technology and piezoelectric properties," *J. Appl. Phys.*, vol. 116, no. 3, 2014.

[8] T. Van Hemert, K. Reimann, and R. J. E. Hueting, "Extraction of second order piezoelectric parameters in bulk acoustic wave resonators," *Appl. Phys. Lett.*, vol. 100, no. 23, 2012.

[9] T. Herzog, S. Walter, and H. Heuer, "Investigations on aluminum nitride thin film properties and design considerations for smart high frequency ultrasound sensors," *... Int. Conf. Sens. ...*, no. c, pp. 129–134, 2011.

[10] M. Zhang, J. Yang, C. Si, G. Han, Y. Zhao, and J. Ning, "Research on the piezoelectric properties of AlN thin films for MEMS applications," *Micromachines*, vol. 6, no. 9, pp. 1236–1248, 2015.

[11] J. Hernando, J. L. Sánchez-Rojas, S. González-Castilla, E. Iborra, A. Ababneh, and U. Schmid, "Simulation and laser vibrometry characterization of piezoelectric AlN thin films," *J. Appl. Phys.*, vol. 104, no. 5, p. 053502, 2008.

[12] T. L. Jordan and N. Langley, "Piezoelectric Ceramics Characterization," *Contract*, p. 23, 2001.

[13] S. Hyunchang, "Piezoelectric Coefficient Measurement of AlN Thin Films at the Nanometer Scale using Piezoresponse Force Microscopy," *J. Korean Phys. Soc.*, vol. 56, no. 2, p. 580, 2010.

[14] A. Ababneh *et al.*, "c-axis orientation and piezoelectric coefficients of AlN thin films sputter-deposited on titanium bottom electrodes," *Appl. Surf. Sci.*, vol. 259, pp. 59–65, 2012.

[15] M.-A. Dubois and P. Muralt, "Measurement of the effective transverse

piezoelectric coefficient e31,f of AlN and Pb(Zrx,Ti1−x)O3 thin films," *Sensors Actuators A Phys.*, vol. 77, no. 2, pp. 106–112, Oct. 1999.
[16] V. Lindroos, *Handbook of silicon based MEMS materials and technologies*. William Andrew/Elsevier, 2010.
[17] G. G. Stoney, "The Tension of Metallic Films Deposited by Electrolysis," *Proc. R. Soc. A Math. Phys. Eng. Sci.*, vol. 82, no. 553, pp. 172–175, May 1909.
[18] M. Chekchaki, V. Lazarus, and J. Frelat, "Analytical and 3D Finite Element Study of the Deflection of an Elastic Cantilever Bilayer Plate," *J. Appl. Mech.*, vol. 78, no. 1, p. 011008, 2011.
[19] M. A. Hopcroft, W. D. Nix, and T. W. Kenny, "What is the Young's Modulus of Silicon?," *J. Microelectromechanical Syst.*, vol. 19, no. 2, pp. 229–238, Apr. 2010.
[20] "PDV-100 Portable Digital Vibrometer Truly Portable Laser Vibration Measurement Datasheet," 2018.
[21] A. Ababneh, U. Schmid, J. Hernando, J. L. Sánchez-Rojas, and H. Seidel, "The influence of sputter deposition parameters on piezoelectric and mechanical properties of AlN thin films," *Mater. Sci. Eng. B*, vol. 172, no. 3, pp. 253–258, 2010.
[22] F. Medjani, R. Sanjinés, G. Allidi, and A. Karimi, "Effect of substrate temperature and bias voltage on the crystallite orientation in RF magnetron sputtered AlN thin films," *Thin Solid Films*, vol. 515, no. 1, pp. 260–265, 2006.
[23] M.-A. Dubois and P. Muralt, "Stress and piezoelectric properties of aluminum nitride thin films deposited onto metal electrodes by pulsed direct current reactive sputtering," *J. Appl. Phys.*, vol. 89, no. 11, p. 6389, 2001.
[24] M. Ishihara, S. . Li, H. Yumoto, K. Akashi, and Y. Ide, "Control of preferential orientation of AlN films prepared by the reactive sputtering method," *Thin Solid Films*, vol. 316, no. 1–2, pp. 152–157, 1998.
[25] H. Cheng, T. Lin, and W. Chen, "Preparation of w 0 0 2 x oriented AlN thin films by mid frequency reactive sputtering technique," vol. 425, pp. 85–89, 2003.
[26] X.-H. Xu, H.-S. Wu, C.-J. Zhang, and Z.-H. Jin, "Morphological properties of AlN piezoelectric thin films deposited by DC reactive magnetron sputtering," *Thin Solid Films*, vol. 388, no. 1, pp. 62–67, 2001.
[27] "PSV-500 Scanning Vibrometer PSV-500 Scanning Vibrometer Full-field vibration measurement Datasheet," 2018.
[28] U. von Wagner and P. Hagedorn, "Nonlinear Effects of Piezoceramics Excited by Weak Electric Fields," *Nonlinear Dyn.*, vol. 31, no. 2, pp. 133–149, 2003.